Wideband Compact Magnetic Antennas Based on Interdigitated Near-Field Resonant Parasitic Elements

Xiaoming Chen[1], Ming-Chun Tang[1],
[1]College of Communication Engineering
Chongqing University
Chongqing, China
cxm849895231@126.com, tangmingchun@cqu.edu.cn

Richard W. Ziolkowski[2]
[2] Global Big Data Technologies Centre
University of Technology Sydney
Ultimo NSW 2007, Australia
richard.ziolkowski@uts.edu.au

***Abstract* - Several compact antennas based on interdigitated magnetic-based near-field resonant parasitic (NFRP) elements are presented. The interdigitated NFRP elements, driven by dipole element, are investigated first to demonstrate that they can facilitate a combination of two adjacent resonant modes which leads to stable radiating performance characteristics. Based on this interdigitated NFRP element, linearly (LP) and circularly (CP) polarized versions are demonstrated. The LP version achieves a 14.9%, –10-dB fractional impedance bandwidth (FBW) along with a stable realized gain ~ 6.7 dBi over this entire frequency range. Similarly, the CP version achieves an 8.13% 3-dB axial ratio (AR) FBW along with a stable realized gain ~ 6.5 dBi over its entire bandwidth. These compact NFRP antennas can be applied to many space-limited wireless communication systems.**

I. INTRODUCTION

Generally, the minimum quality factor for a magnetic electrically small antenna (ESA) is a factor of two larger than an electric one with the same electric size [1]. Hence, magnetic ESAs usually exhibit about half the bandwidth when compared with electric ones. In order to promote their potential applications for wideband space-limited platforms, several approaches have been undertaken to expand their bandwidths. For example, multiple near-field resonant parasitic (NFRP) elements [2], [3] and active elements [4], [5] have been successfully employed to expand their bandwidths. In this paper, different from the above two methods, we shall introduce several bandwidth-enhanced magnetic ESA designs arising from their interdigitated NFRP elements.

II. BANDWIDTH-ENHANCED MAGNETIC-BASED NFRP ESA

Fig. 1(a) details the geometry of our interdigitated magnetic-based NFRP ESA. It consists of a driven dipole element and an interdigitated magnetic NFRP element. Different from the classical NFRP ESA which has an intact magnetic NFRP element [6], i.e., a simple capacitively-loaded loop (CLL) with a single gap, the NFRP element in this wideband design has evolved into an eight-unit interdigitated version. The dimensions and placement of the driven dipole are adjusted in order to maximize the coupling between the driven element and the interdigitated NFRP elements [7], [8]. The multiple fingers of the interdigitated units enhance their capacitance. These increased capacitances, together with an increased length of the driven dipole, facilitate the excitation of both the fundamental and first higher order modes of the antenna. Their values can be tailored to low the ratio of these two resonance frequencies.

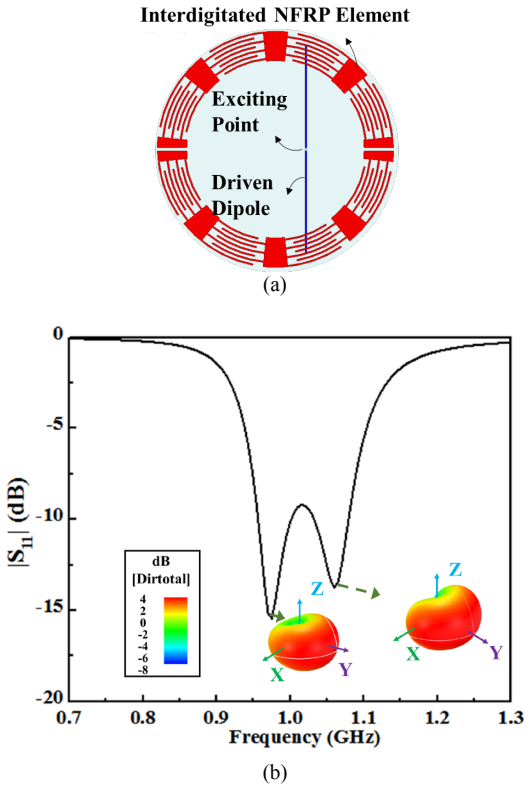

Fig. 1. Dipole-driven, interdigitated NFRP ESA. (a) Configuration. (b) Simulated $|S_{11}|$ values. The 3-D directivity radiation patterns are also indicated at the two resonances.

Fig. 1(b) gives the simulated reflection coefficient ($|S_{11}|$) values of this dipole-driven, interdigitated NFRP ESA. It is readily seen that there are two adjacent resonance frequencies, i.e., 0.97 and 1.06 GHz, and that they significantly overlap to exhibit a wide 9.1% fractional bandwidth (FBW). The electrical size of this innovative ESA is ka = 0.80. The simulated 3-D directivity patterns at those two resonance frequencies are also given. It is readily seen that the radiation

performance at these two resonance frequencies is quite similar. In fact, the pattern performance is found to be stable over its entire operational bandwidth [9].

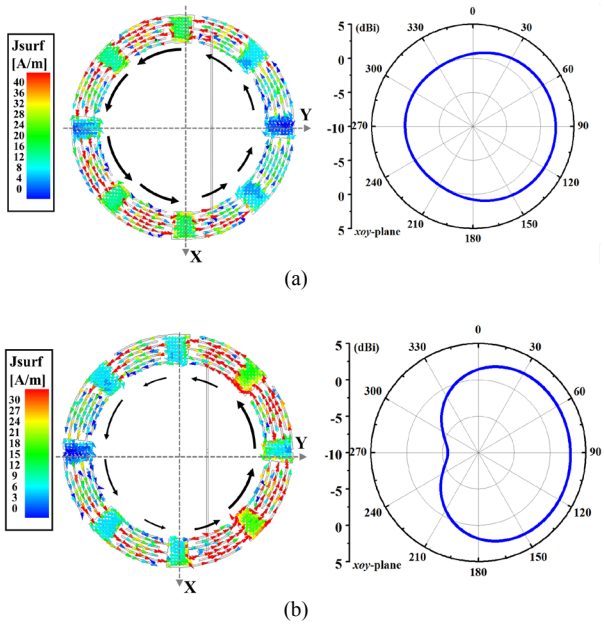

Fig. 2. Surface current distributions on the interdigitated NFRP elements and the 2-D directivity patterns in the *x0y*-plane at two resonance frequency points. (a) @ 0.97 GHz. (b) @ 1.06 GHz.

Figs. 2(a) and 2(b) show, respectively, the surface current distributions on the interdigitated NFRP element and the resulting 2-D directivity pattern in the *x0y*-plane. Even though the magnitudes of the currents on the periodic interdigitated NFRP element at the lower frequency, 0.97 GHz, presented in Fig. 2(a) are slightly asymmetric with respect to the *x*-axis, they are still operating in its fundamental mode. Viewing the *+y* half of the interdigitated NFRP element as an electric dipole and its *–y* half as one whose current direction is opposite, the antenna is in a quasi-Yagi configuration [7], [8]. In particular, the *–y* half acts as the reflector, and the +y half acts as the director. Considering that the magnitudes of surface currents on the –y-half are larger than those on the +y half, the directivity pattern points towards the +y half with a front-to-back ratio (FTBR) value of 2.2 dB. The surface currents shown in Fig. 2(b) at the higher resonance frequency, 1.06 GHz, resemble an anti-phase first higher order mode. They are concentrated more on the *+y* side of the interdigitated NFRP element, but with higher amplitudes now on its *–y* side. Thus, the fields radiated by this quasi-Yagi configuration are again pointed primarily in the *+y* direction, but they are stronger than those at the lower resonance frequency [7]. This behavior yields a larger FTBR value, 8.5 dB.

III. Wideband NFRP LP and CP Designs

A. LP Prototype

The monopole-driven, linearly polarized (LP) antenna with its innovative interdigitated NFRP element is proposed and shown in Fig. 3(a) based on the former ESA. In contrast to the proposed ESA in Fig. 1, the magnetic NFRP element is divided in half and is oriented perpendicular to and in the center of a large circular metal ground.

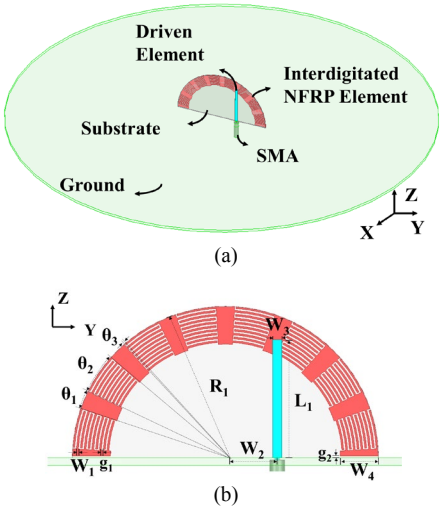

Fig. 3. The LP NFRP antenna configuration. (a) 3-D isometric view. (b) Side view in the *y0z* plane. (g_1 = 0.5 mm, g_2 = 0.5 mm, L_1 = 31.2 mm, W_1 = 0.5 mm, W_2 = 13.5 mm, W_3 = 0.6 mm, W_4 = 10.0 mm, R_1 = 0 mm, θ_1 = 7.0º, θ_2 = 15.5 º, θ_3 = 0.5 º)

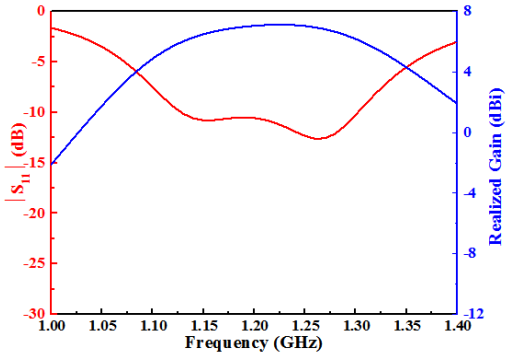

Fig. 4. Simulated performance characteristics ($|S_{11}|$ and realized gain values) of the LP prototype.

The simulated $|S_{11}|$ values of the LP prototype together with its realized gain values are presented in Fig. 4. It indicates that the antenna exhibits a wide –10-dB bandwidth from 1.12 to 1.30 GHz, corresponding to a 14.9% FBW. This result is much wider than the corresponding one with its simple, intact CLL NFRP element (~2.9%). The two resonance frequency points anticipated from Fig. 1 are clearly seen. The total electric size of the magnetic NFRP element, which is the main radiator of this antenna, is *ka* = 0.921 at the lower frequency bound of its operational bandwidth. The simulated boresight realized gain values are maintained near 6.7 dBi across that operational band. The simulated radiation efficiency (RE) values are higher than 95% over the entire band.

B. CP Prototype

Based on the LP one, two orthogonal, vertically oriented interdigitated NFRP elements with a simple feed network are combined to achieve a circularly polarized (CP) antenna. Fig. 5(a) provides an isometric view of this CP configuration. Note that the feed structure is orthogonal and symmetrical with respect to the 45° plane as illustrated in Fig. 5(b). Figs. 5(c) and 5(d) show that each interdigitated NFRP element is similar to the LP design in Fig. 3.

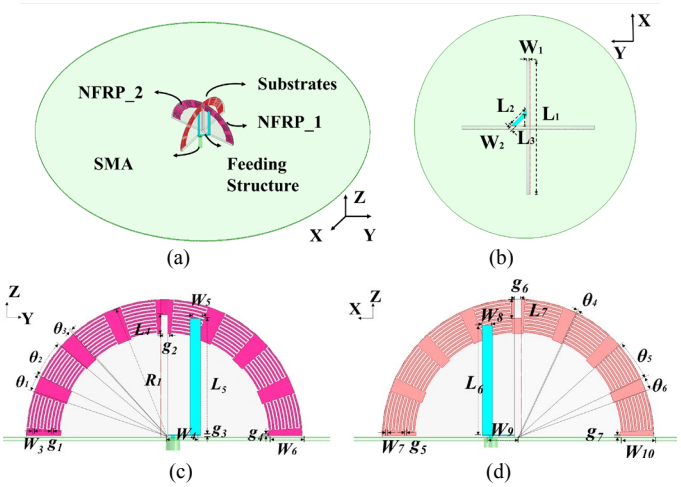

Fig. 5. The geometry of the CP monopole-driven IDC-based NFRP antenna. (a) 3D isometric view. (b) Top view. (c) Side view of the *y0z*-plane cut. (d) Side view of the *z0x*-plane cut. (Lengths in millimeters: $g_1 = 0.56$, $g_2 = 2.0$, $g_3 = 0.5$, $g_4 = 0.5$, $g_5 = 0.54$, $g_6 = 2.0$, $g_7 = 0.5$, $L_1 = 80.0$, $L_2 = 12.2$, $L_3 = 5.6$, $L_4 = 5.5$, $L_5 = 34.4$, $L_6 = 32.4$, $L_7 = 5.5$, $R_1 = 40.0$, $W_1 = 0.508$, $W_2 = 0.28$, $W_3 = 0.44$, $W_4 = 8.9$, $W_5 = 0.25$,$W_6 = 10.0$, $W_7 = 0.46$, $W_8 = 0.12$, $W_9 = 8.9$, $W_{10} = 10.0$. Angles in degrees: $\theta_1 = 5.7$, $\theta_2 = 16.8$, $\theta_3 = 0.5$, $\theta_4 = 0.5$, $\theta_5 = 16.0$, $\theta_6 = 6.5$)

The simulated performance characteristics results shown in Fig. 6(a) indicate that the antenna exhibits a wide –10-dB impedance bandwidth from 1.08 to 1.24 GHz, corresponding to a fractional bandwidth of 13.8%. The realized gain values are quite stable (~6.5 dBi) and the *RE* values are greater than 88% over the entire operational bandwidth. Fig. 6(b) demonstrates that the associated 3-dB AR bandwidth is from 1.12 to 1.215 GHz, corresponding to a fractional bandwidth of 8.13% [5]. This bandwidth is substantially wider than the ~1.5% value of the original CLL NFRP CP antenna [10]. The electric size of the NFRP radiating element is $ka = 0.923$ corresponding to the lower frequency bound of the 3-dB AR bandwidth.

IV. Conclusion

In this paper, several wideband metamaterial-inspired, NFRP antennas are introduced in this work. The interdigitated NFRP element was first introduced to cooperate with an ideal dipole-driven magnetic ESA design. A five-fold impedance bandwidth enhancement was demonstrated. Both LP and CP versions of monopole-driven, interdigitated-CLL NFRP antennas were successfully designed. These compact NFRP antennas can be extensively applied in space-limited wireless communication systems in the near future.

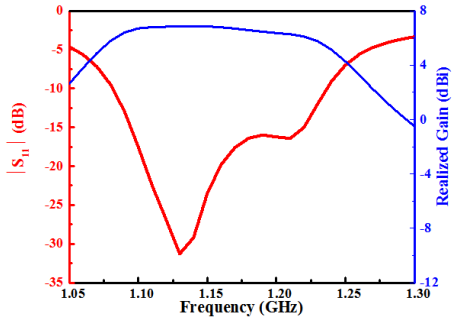

Fig. 6. Simulated results of the CP monopole-driven, NFRP antenna prototype. (a) $|S_{11}|$ values and realized gain values. (b) AR values.

References

[1] H. L. Thal, "New radiation limits for spherical wire antennas," *IEEE Trans. Antennas Propag.*, vol. 54, no. 10, pp. 2757–2763, Oct. 2006.

[2] M.-C. Tang, Y. Chen, T. Shi and R. W. Ziolkowski, "Bandwidth-enhanced, compact, near-field resonant parasitic filtennas with sharp out-of-band suppression," *IEEE Antennas Wireless Propag. Lett.*, vol. 17, no. 8, pp. 1483–1487, Aug. 2018.

[3] M.-C. Tang, X. Chen, M. Li, and R. W. Ziolkowski, "Particle swarm optimized, 3-D-printed, wideband, compact hemispherical antenna," *IEEE Antennas Wireless Propag. Lett.*, vol. 17, no. 11, pp. 2031–2035, Nov. 2018.

[4] M.-C. Tang, and R. W. Ziolkowski, "Frequency-agile, efficient, near-field resonant parasitic monopole antenna," *IEEE Trans. Antennas Propag.*, vol. 62, no. 3, pp. 1479–1483, Mar. 2014.

[5] M.-C. Tang, and R. W. Ziolkowski, "Frequency-agile, efficient, circularly polarized, near-field resonant antenna: designs and measurements," *IEEE Trans. Antennas Propag.*, vol. 63, no. 11, pp. 5203–5209, Nov. 2015.

[6] P. Jin and R. W. Ziolkowski, "Metamaterial-inspired, electrically small Huygens sources," *IEEE Antennas Wireless Propag. Lett.*, vol. 9, pp. 501–505, 2010.

[7] M.-C. Tang, B Zhou, Y. Duan, X. Chen, and R. W. Ziolkowski, "Pattern-reconfigurable, flexible, wideband, directive, electrically small near-field resonant parasitic antenna," *IEEE Trans. Antennas Propag.*, vol. 66, no. 5, pp. 2271-2280, 2018.

[8] M.-C. Tang, B. Zhou, and R. W. Ziolkowski, "Flexible uniplanar electrically small directive antenna empowered by a modified CPW-feed," *IEEE Antennas Wireless Propag. Lett.*, vol. 15, pp. 914-917, 2016.

[9] K. -Z. Hu, M.-C. Tang, M Li, R.W. Ziolkowski, "Compact, low-profile, bandwidth-enhanced substrate integrated waveguide filtenna," *IEEE Antennas Wireless Propag. Lett.*, vol. 17, no. 8, pp. 1552-1556, 2018.

[10] P. Jin and R. W. Ziolkowski, "P. Jin and R. W. Ziolkowski, "Multi-frequency, linear and circular polarized, metamaterial-inspired near-field resonant parasitic antennas," IEEE Trans. Antennas Propag., vol. 59, pp. 1446-1459, May 2011.